

Optical Properties of Low-Defect Large-Area Hexagonal Boron Nitride for Quantum Applications

Shrivatch Sankar, Shantanu Saha, Jia-Shiang Chen, Shih-Po Chien, Yann-Wen Lan, Xuedan Ma, Michael Snure, and Shamsul Arafin*

Intrinsic defects and their concentrations in hexagonal boron nitride (h-BN) play a key role in single-photon emission. In this study, the optical properties of large-area multilayer h-BN-on-sapphire grown by metal-organic chemical vapor deposition are explored. Based on the detailed spectroscopic characterization using both cathodoluminescence (CL) and photoluminescence (PL) measurements, the material is devoid of random single-point defects instead of a few clustered complex defects. The emission spectra of the measurements confirm a record-low-defect concentration of $\approx 10^4 \text{ cm}^{-2}$. Post-annealing, no significant changes are observed in the measured spectra and the defect concentrations remain unaltered. Through CL and PL spectroscopy, an optically active boron vacancy spin defect is identified and a novel complex defect combination arising from carbon impurities is revealed. This complex defect, previously unreported, signifies a unique aspect of the material. In these findings, the understanding of defect-induced optical properties in h-BN films is contributed, providing insights for potential applications in quantum information science.

technologies and integrated quantum photonics due to hosting of single-photon emitters (SPEs).^[1,2] Color centers in h-BN have generated a spark for fundamental research to understand the potential of this ultrawide bandgap semiconductor ($\approx 6 \text{ eV}$). Unlike graphene, h-BN is a suitable 2D material for bandgap engineering. It is a good host of point defects spanning from ultraviolet (UV) to near-infrared, which makes it a versatile material to be used for both optoelectronic and quantum devices.^[1–5] Point defects in h-BN, including vacancies, interstitials, adatoms, substitutions, dopant atoms, and antisites, introduce new energy levels within the bandgap, leading to novel optical properties including SPEs. Typically, these defects arise during the growth process or from external sources such as electron, ion, and particle irradiation.^[6] To achieve

1. Introduction


White graphene, also known as hexagonal boron nitride (h-BN) is a van der Waals material that has shown unprecedented scientific and technological breakthroughs for quantum information

better control over the linewidth and brightness of SPEs from these defects, it is important to address the challenges posed by structural imperfections resulting from the defect creation process. This is resolved by introducing point defects in a controllable manner through precise defect engineering.^[7]

S. Sankar, S. Arafin
Department of Electrical and Computer Engineering
The Ohio State University
Columbus, OH 43210, USA
E-mail: arafin.1@osu.edu

S. Saha
Department of Electrical, Electronics and Communication Engineering
GITAM School of Technology
GITAM (Deemed to be University)
Hyderabad, Telangana 502329, India

J.-S. Chen, X. Ma
Center for Nanoscale Materials
Argonne National Laboratory
Lemont, IL 60439, USA

 The ORCID identification number(s) for the author(s) of this article can be found under <https://doi.org/10.1002/pssr.202400034>.

© 2024 The Authors. physica status solidi (RRL) Rapid Research Letters published by Wiley-VCH GmbH. This is an open access article under the terms of the Creative Commons Attribution License, which permits use, distribution and reproduction in any medium, provided the original work is properly cited.

DOI: 10.1002/pssr.202400034

J.-S. Chen, X. Ma
Center for Molecular Quantum Transduction
Northwestern University
Evanston, IL 60208, USA

S.-P. Chien, Y.-W. Lan
Department of Physics
National Taiwan Normal University
Taipei 116, Taiwan

X. Ma
Consortium for Advanced Science and Engineering
University of Chicago
Chicago, IL 60637, USA

M. Snure
Air Force Research Laboratory
Sensors Directorate
Wright-Patterson AFB, OH 45433, USA

To determine the repeatability and scalability of SPEs, a comprehensive understanding of the defect density and luminescence properties of h-BN is essential. While there are numerous reports on the luminescence properties of bulk h-BN,^[8–12] only a few have delved into the luminescence properties of monolayer (ML) to few-layer 2D h-BN. In the realm of 2D h-BN, extensive research has focused on the optical properties of exfoliated h-BN.^[13–15] Unfortunately, exfoliated h-BN has limitations, such as smaller-area coverage, irregular thicknesses, and highly nonuniform defect distributions concentrated at wrinkles, grain boundaries, and flake edges. Furthermore, challenges arise when depositing tape-exfoliated crystals over large areas, as they typically exist as few tens of micrometer-sized flakes. This highlights the importance of investigating large-area h-BN. Numerous efforts have been made to investigate the optical properties of large-area h-BN thin films using CL and PL.^[16] So far, researchers have primarily focused on characterizing defect-rich h-BN. Low-defect (or defect-free) h-BN, however, has not yet been much explored as quantum materials. Understanding the optical properties of low-defect h-BN is essential for defect engineering, such as intercalated foreign-atom-based deterministic quantum light sources and next-generation electronic devices.^[17,18] While the investigations of SPE densities have been reported, a comprehensive analysis of the defect density pertaining to all optically active defects remains lacking.

In this article, we report the spectroscopic characterization of h-BN films grown on sapphire substrates. Our CL and PL studies reveal that the material possesses a low density of optically active defects. Based on PL spatial mapping, defect density is measured to be 10^4 cm^{-2} . This is significantly lower than the previously reported values, which were in the range of 10^8 – 10^{10} cm^{-2} .^[19,20] Additionally, room-temperature (RT)

CL and PL analysis reveals the presence of optically active boron vacancy- and carbon-based defects within the material.

2. Experimental Section

Six-ML (2 nm) h-BN films were grown on top of sapphire substrates using metal-organic chemical vapor deposition (MOCVD) at a growth temperature of 1100 °C. Growth details can be found elsewhere.^[21] **Figure 1a** shows the Nomarski image of the h-BN thin films, indicating its uniformity and absence of any inhomogeneity. In **Figure 1b**, atomic force microscopy (AFM) reveals a smooth surface with a surface roughness of 1.1 Å. Both Nomarski and AFM images confirm that the sample is free from any protrusions or wrinkles. The smooth surface morphology also indicates that the h-BN films lack in-plane strain, suggesting excellent lattice matching between h-BN and sapphire during the growth process.^[22,23] X-ray photoelectron spectroscopy (XPS) was performed on the sample, and the results are shown in **Figure 1c**. The XPS data collected showed the boron and nitrogen signals, closely resembling the stoichiometry of h-BN. In addition to B and N, the material contained Al, O, and C atoms. While Al and O were attributed to the substrate, the significant presence of C atoms was likely due to impurities that might have arisen during the growth process, possibly from the use of the triethylborane (TEB) precursor. Raman measurements were conducted on this sample to assess its vibrational properties and the quality of the h-BN films. The characteristic E_{2g} phonon mode peak of h-BN at 1370 cm^{-1} with a full width at half maximum (FWHM) of 22.8 cm^{-1} was recorded, as shown in **Figure 1d**. The measured FWHM still

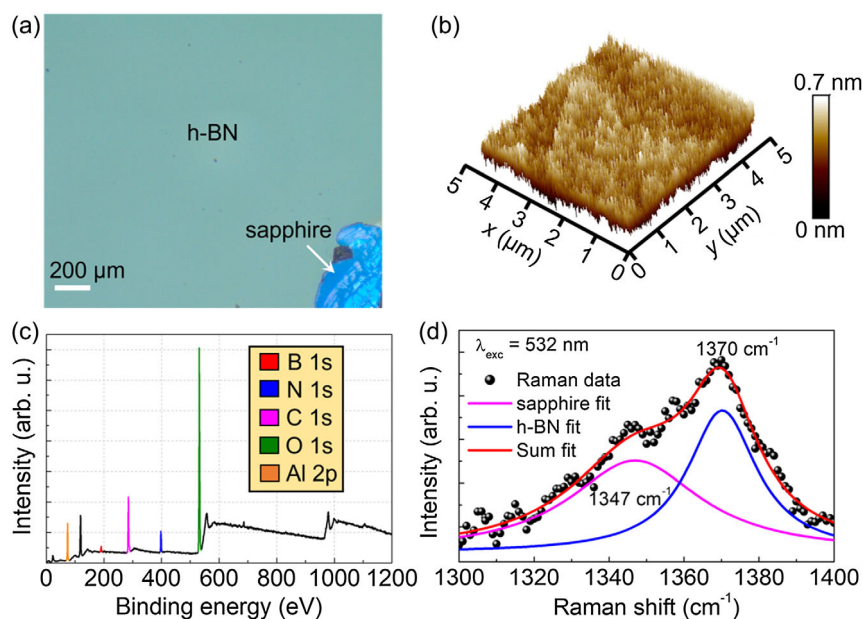


Figure 1. a) Optical microscope (Nomarski) image of h-BN on sapphire substrates with a scratch on the bottom-right to distinguish between h-BN and sapphire, b) AFM image of the h-BN/sapphire, covering an area of $5 \times 5 \mu\text{m}^2$, c) survey XPS spectrum, and d) Raman spectra of the E_{2g} phonon mode peak of h-BN with an FWHM of 22.8 cm^{-1} .

appeared slightly broader compared to exfoliated flakes due to the use of sapphire substrates.^[24] This broader FWHM was primarily attributed to the interference of sapphire's phonon peak at 1347 cm^{-1} , which we attempted to suppress by reducing the laser excitation power density but still seems to be dominant. Nevertheless, the measured FWHM was still superior in contrast to most h-BN films grown on sapphire in terms of crystallinity.^[25–28]

Raman measurements were performed using Andor Kymera 328i spectrograph with a DR-316B-LDC-DD-RES detector equipped with a 532 nm excitation source at 8.95 mW. The measurements utilized a 0.75 numerical aperture (NA) $50\times$ objective, a grating of 1200 L mm^{-1} , a spot size of $1.3\text{ }\mu\text{m}$, and an exposure time 5 s. CL measurement was carried out using Thermo Scientific's Quattro environmental scanning electron microscope with a Delmic SPARC CL detector. The CL excitation was chosen from 200 to 5 kV with a beam current from 28 pA to 0.11 nA. The CL spectra were collected by integrating over the mapped area of $1\times 1\text{ }\mu\text{m}^2$, with each pixel being 100 nm and an integration time of 100 ms. A 440 nm excitation laser was used in continuous-wave mode with an excitation power of $127\text{--}255\text{ W cm}^{-2}$ for PL measurements. PL mapping and PL lifetime measurements were carried out at excitation power from 5 to 13 W cm^{-2} . An objective lens with $40\times$ magnification and an NA of 0.95 was used to focus the laser beam onto the sample, resulting in a beam spot size of $1\text{ }\mu\text{m}$. PL spectra were measured using a spectrometer with a spectral resolution of 0.26 nm, and integration times of 60 s, while PL mapping was performed at 5 ms pixel^{-1} .

For the PL lifetime measurements, a pulsed laser beam at 440 nm with a 10 MHz repetition rate, 20 ps pulse duration, and pulse-to-pulse jitter 2.6 ps was focused onto the sample. PL emission from the sample was collected by the same objective and spectrally filtered by a combination of longpass filters with a cutoff at 475 and 495 nm. The collected PL was then split by a 50:50 beam splitter and focused onto two single-photon counting detectors with a Hanbury–Brown and Twiss (HBT) geometry for the time-resolved PL (TRPL). Additionally, photon correlation measurements were conducted using time-correlated photon counting

electronics (PicoQuant). The pristine sample was annealed at a temperature of 1123 K for 30 min in an argon (Ar) atmosphere on an Across International 150 mm Furnace Tube.

3. Results and Discussions

3.1. CL Analysis

During the initial measurements at 5 kV CL excitation, we observed only the luminescence peaks of sapphire at 375 nm (3.3 eV), 696 nm (1.78 eV), and 752 nm (1.65 eV), as shown in Figure 2a. These defects are attributed to the presence of F_2^+ , Cr^{3+} , and Ti^{3+} centers in the sapphire substrates.^[29] Typically, high CL excitation was used to characterize a few layered 2D materials when they were placed on a transmission electron microscopy grid, isolating the sample from the substrate's luminescence. Since the six-ML h-BN under study were grown on the luminescent bright oxide substrates, we deliberately reduced the CL excitation so that the electron beam did not reach the substrates. This prevents the fluorescence emitted by the defect peaks in the substrate from overshadowing the point defect spectrum of the h-BN. It was determined that the optimal CL excitation voltage for the 2 nm films was approximately 200 V. However, the signal-to-noise ratio in CL detection was notably low for CL excitation voltages between 200 and 950 V. Therefore, the CL excitation voltage was increased to 1 kV.

The resulting CL spectra reveal the same substrate luminescent peaks at 381 nm (3.25 eV) and 763 nm (1.62 eV), even at 1 kV, as illustrated in Figure 2b. In addition, another luminescent broad peak also appears at 880 nm. This peak is associated with the negatively charged optically spin active boron vacancy center (V_B^-). The unique optical properties of the V_B^- center, including its luminescent emission at 880 nm, were previously reported.^[30] The broadening of the lineshape could be due to the deviation in orientation of the atomic planes that are parallel to each other, strong electron–phonon coupling, and the Jahn–Teller effects.^[31] Furthermore, these findings suggest that the boron vacancy V_B^- defect center undergoes a spin-dependent intersystem crossing pathway within the system.

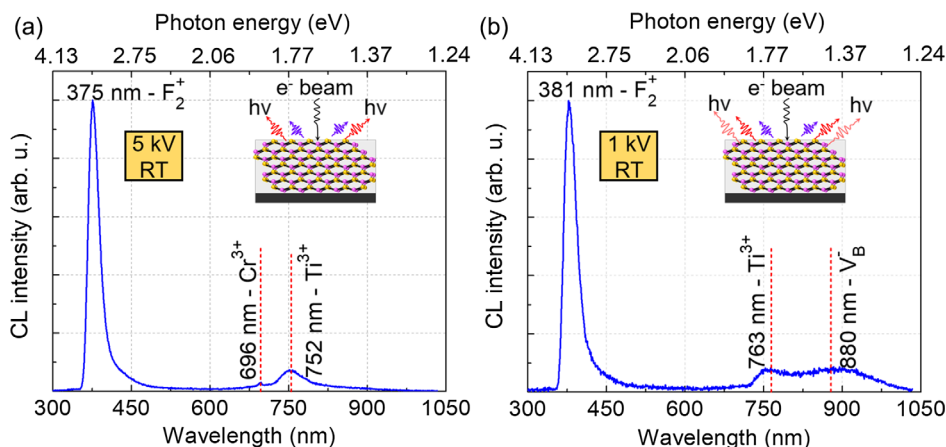


Figure 2. RT CL spectrum of the h-BN/ sapphire sample excited with the CL excitation voltages at a) 5 kV and b) 1 kV.

This phenomenon preserves the orbital singlet, and triplet spin nature of the V_B^- arising from spin–spin interaction, providing intriguing opportunities for exploring quantum coherence and spin-related effects in h-BN.^[32] The negatively charged vacancy center in h-BN is commonly generated through exposure to high-energy electron irradiation, ion irradiation, and intense laser beams.^[33–35] In our case, the sample was not exposed to any of these conditions. Therefore, the possible reason for this defect origin could be intrinsic, originating during the growth process. Due to the difficulties arising from the strong substrate’s fluorescence and limitations in mapping the defect peak caused by the CL excitation voltage and CL detection system, PL experiments were performed to obtain further insights of the material.

3.2. PL Analysis

The PL measurement reveals two luminescent defect peaks around 521 nm (2.38 eV) with a shoulder peak at 574 nm (2.16 eV) as shown in Figure 3a. The zero-phonon line (ZPL)-based emissions were reported earlier within a range from 1.56 to 2.27 eV.^[36–38] However, the emission at 2.38 eV in our material is less likely to be ZPL as it does not fall within that range. Moreover, the energy difference between these two peaks is around 231 meV, which also rules out the possibility of phonon sideband (PSB)-based emissions from 2.16 eV.^[37] The broad emissions from these two peaks attribute to the clustering of point defects forming a single large clustered or an embedded

point defect. HBT measurements were conducted on to confirm the presence of defect clustering. The antibunching factor $g^2(0)$ value was measured to be 0.88 as shown in Figure 3b, implying that more than one point defect contributes to this $g^2(0)$ value, confirming the presence of cluster defects. TRPL measurements were also conducted to study the fluorescence lifetime of the defects. The PL lifetimes measure to be 1.8 ns for the 521 nm peak and 1.5 ns for the 574 nm peak, both exhibiting biexponential decay with time constants ($\tau_1 = 4.8$ ns, $\tau_2 = 1.1$ ns and $\tau_1 = 4.2$ ns, $\tau_2 = 1$ ns) displayed in Figure 3c. Based on the PL lifetime, the observed defects exhibit a shorter lifetime when compared to SPEs reported in the same wavelength range.^[38–40]

To study the thermal stability of these defects, the pristine sample was annealed at a temperature of 850 °C in an Ar atmosphere for 30 min. In general, annealing activates defects that were initially not optically-active and can also annihilate large defect clusters, isolating single-point defects. However, in our case, defect annihilation was not observed; instead, optical activation of a defect was observed. The annealed sample exhibits a new PL peak at 890 nm from the defect cluster which is attributed to the V_B^- center, as shown in Figure 3d. HBT measurement results of the annealed sample were found similar to the pristine sample with a $g^2(0)$ value of 1, as shown in Figure 3e, suggesting that these clustered defects are prone to withstand high temperatures without losing their emission properties. Interestingly, an increase in the lifetime of the defects is observed, as shown in Figure 3f. The lifetime of the 522 nm peak is 3 ns, the 575 nm peak has a lifetime of 2.6 ns, and the 890 nm peak exhibits a

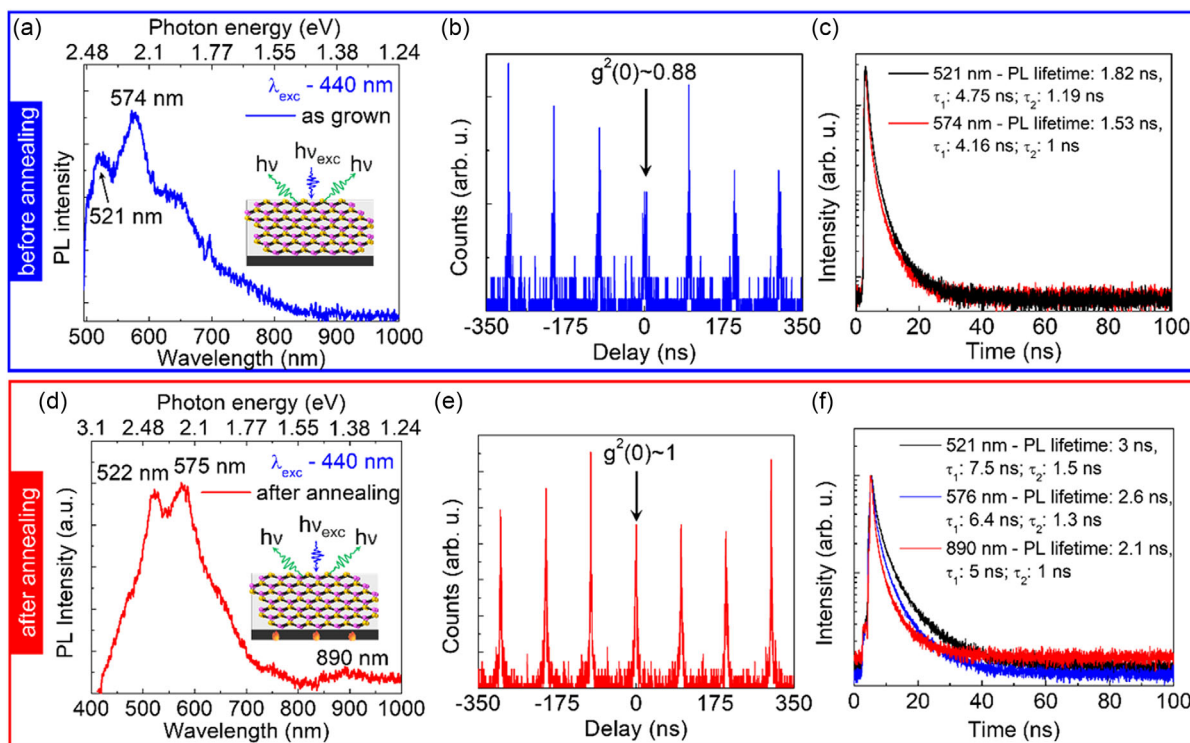


Figure 3. a,d) RT-PL spectra; b,e) second-order autocorrelation data; and c,f) PL lifetime of the pristine h-BN/sapphire (top row) and annealed samples (bottom row).

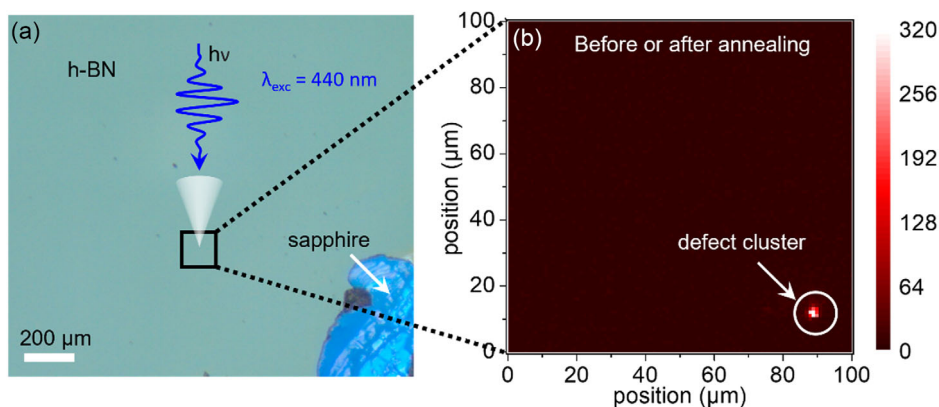


Figure 4. a) Optical microscopic image of the sample and b) spatial PL mapping of the h-BN sample before and after annealing.

lifetime of 2.1 ns. These three peaks demonstrate biexponential decay with time constants ($\tau_1 = 7.5$ ns, $\tau_2 = 1.5$ ns; $\tau_1 = 6.4$ ns, $\tau_2 = 1.3$ ns; and $\tau_1 = 5$ ns, $\tau_2 = 1$ ns). These lifetime values were found to be consistent with the previously reported SPEs, even though the defects were not SPEs.^[38–40]

There are numerous reports on the defect emissions in the range of 1.9–2.4 eV that are associated with the presence of carbon impurities in h-BN.^[39,41,42] Taking that into account, by analyzing the emission spectra presented in Figure 3d, it is evident that the sample includes complex defect clusters featuring the boron vacancy center and carbon-based defects. The incorporation of carbon into our material can occur during the growth process, facilitated by the use of the TEB precursor. Carbon typically introduces impurities in h-BN by substituting either a boron atom (C_B) or a nitrogen atom (C_N). However, previous reports have attributed individual PL emission peaks (521 and 575 nm) to different types of defect formations like $V_B C_N^-$, $C_B C_N$, and $C_B C_N$ dimer.^[39,41,42] The specific combination of a peak at 522 nm followed by a shoulder peak at 575 nm was not reported by other studies, except for Jara et al. leading us to speculate the defect in our material could be related with $C_N^- - C_B^+ - 3$ where both boron and nitrogen atoms were substituted.^[43] Interestingly, a defect cluster comprising C_N , C_B , and V_B^- center with emission wavelengths around 522 nm, 575 nm, and 890 nm has not yet been reported elsewhere. Therefore, it is assumed that the defect in our material could be a new type of complex triplet-site defect cluster comprising C_N , C_B , and V_B^- , which will be investigated in our future research to understand its defect chemistry.

3.3. Measurement of Defect Density

In both CL and PL experiments, we observe the presence of various defect peaks within our h-BN sample. This observation led us to quantify the defect densities in the material. To detect these defects, we conducted high-resolution RT PL mapping. Multiple PL mappings were performed over a substantial 1 cm^2 area of the h-BN sample, with each scan covering a $100 \times 100 \mu\text{m}^2$ region, as illustrated in Figure 4a. Our analysis, based on multiple PL mappings of both as-grown and annealed samples, reveals the presence of only one defect cluster per scan area, as shown in Figure 4b. This analysis results in an optically

active defect density of approximately 10^4 cm^{-2} . These findings confirm that the h-BN sample has a low optically active defect density. Notably, our determined defect densities in the sample are lower than the values reported in previous studies, which were in the range of 10^8 – 10^{10} cm^{-2} .^[19,20]

4. Conclusion

In summary, we present the optical characterization of a large-area h-BN film on sapphire with a low-defect density of 10^4 cm^{-2} . Low-defect materials, being in demand for deterministic SPEs with high stability and purity, were grown in the study by reducing native point defects in the material. The PL analysis confirms the presence of very few carbon-based impurities in the material, attributing to a new type of complex defect cluster comprising $C_N^- - C_B^+ - 3$ and V_B^- . The precise nature of this carbon-based complex defects requires further investigation and will be reported in our future studies. The CL analysis explores the presence of optically spin-active V_B^- defects in the material, a promising development for our upcoming research on rare gas atoms intercalation.^[17] Intercalating h-BN thin films with rare gas atoms represents an underexplored area, particularly when coupling the optically active spin defects from h-BN with the non-nuclear spins of rare gas atoms. This approach has the potential to create stable quantum emitters with high coherence at RT and maintain the quantum entanglement of photons for extended periods.

Acknowledgements

This work was supported in part by The Ohio State University Materials Research Seed Grant Program, funded by the Center for Emergent Materials, an NSF-MRSEC, grant DMR-2011876, the Center for Exploration of Novel Complex Materials, and the Institute for Materials and Manufacturing Research. M.S. acknowledges funding from the Air Force Office of Scientific Research under award no. FA9550-19RYCOR050. J.-S.C. and X.M. acknowledge support from the Center for Molecular Quantum Transduction, an Energy Frontier Research Center funded by the U.S. Department of Energy, Office of Science, Office of Basic Energy Sciences, under award no. DE-SC0021314. Work performed at the Center for Nanoscale Materials, a U.S. Department of Energy Office of Science User Facility, was supported by the U.S. DOE, Office of Basic Energy Sciences, under contract no. DE-AC02-06CH11357.

Conflict of Interest

The authors declare no conflict of interest.

Data Availability Statement

The data that supports the findings of this study are available within the article.

Keywords

cathodoluminescence, clustered point defects, hexagonal boron nitride, low-defect densities, photoluminescence

Received: January 24, 2024

Revised: March 4, 2024

Published online:

- [1] T. T. Tran, C. Elbadawi, D. Totonjian, C. J. Lobo, G. Grosso, H. Moon, D. R. Englund, M. J. Ford, I. Aharonovich, M. Toth, *ACS Nano* **2016**, *10*, 7331.
- [2] R. Bourrellier, S. Meuret, A. Tararan, O. Stéphan, M. Kociak, L. H. G. Tizei, A. Zobelli, *Nano Lett.* **2016**, *16*, 4317.
- [3] X. Li, G. D. Shepard, A. Cupo, N. Camporeale, K. Shayan, Y. Luo, V. Meunier, S. Strauf, *ACS Nano* **2017**, *11*, 6652.
- [4] T. Q. P. Vuong, G. Cassabois, P. Valvin, A. Ouerghi, Y. Chassagneux, C. Voisin, B. Gil, *Phys. Rev. Lett.* **2016**, *117*, 097402.
- [5] B. Shevitski, S. M. Gilbert, C. T. Chen, C. Kastl, E. S. Barnard, E. Wong, D. F. Ogletree, K. Watanabe, T. Taniguchi, A. Zettl, S. Aloni, *Phys. Rev. B* **2019**, *100*, 155419.
- [6] M. Schleberger, J. Kotakoski, *Materials* **2018**, *11*, 1885.
- [7] J. Jiang, T. Xu, J. Lu, L. Sun, Z. Ni, *Research* **2019**, *2019*, 4641739.
- [8] K. Era, F. Minami, T. Kuzuba, *J. Lumin.* **1981**, *24*, 71.
- [9] A. I. Lukomskii, V. B. Shipilo, L. M. Gameza, *J. Appl. Spectrosc.* **1992**, *57*, 607.
- [10] K. Watanabe, T. Taniguchi, H. Kanda, *Nat. Mater.* **2004**, *3*, 404.
- [11] A. V. Kanaev, J.-P. Petit, L. Miseur, V. Marine, V. L. Solozhenko, V. Zafirooulos, *J. Appl. Phys.* **2004**, *96*, 4483.
- [12] L. Miseur, A. Kanaev, *J. Appl. Phys.* **2008**, *103*, 10.
- [13] J. Loyza, J. Barjon, A. Pierret, A. Betz, B. Placais, F. Ducastelle, A. Loiseau, in *Near-band edge optical properties of exfoliated h-BN layers*, Graphene Bilbao, Spain **2013**.
- [14] D. Lee, S. H. Song, *RSC Adv.* **2017**, *7*, 7831.
- [15] S. Choi, T. T. Tran, C. Elbadawi, C. Lobo, X. Wang, S. Juodkazis, G. Seniutinas, M. Toth, I. Aharonovich, *ACS Appl. Mater. Interfaces* **2016**, *8*, 29642.
- [16] A. F. Rigosi, A. L. Levy, M. R. Snure, N. R. Glavin, *J. Phys. Mater.* **2021**, *4*, 032003.
- [17] S. Saha, S. Sankar, S. S. S. Nikor, S. Arafín, *Phys. Status Solidi RRL* **2023**, *2300066*.
- [18] S. Moon, J. Kim, J. Park, S. Im, J. Kim, I. Hwang, J. K. Kim, *Adv. Mater.* **2023**, *35*, 2204161.
- [19] <https://www.2dsemiconductors.com/hexagonal-boron-nitride-h-bn/> (accessed: November 2023).
- [20] Z. Qiu, K. Vaklinova, P. Huang, M. Grzeszczyk, H. Yang, K. Watanabe, T. Taniguchi, K. Novoselov, J. Lu, M. Koperski, Atomic structure of carbon centres in hBN: towards engineering of single photon sources, arXiv:2110.07842 **2021**.
- [21] S. Vangala, G. Siegel, T. Prusnick, M. Snure, *Sci. Rep.* **2018**, *8*, 8842.
- [22] K. Bera, D. Chugh, A. Patra, H. H. Tan, C. Jagadish, A. Roy, *Solid State Commun.* **2020**, *310*, 113847.
- [23] S. Saha, A. Rice, A. Ghosh, S. Hasan, W. You, T. Ma, A. Hunter, L. Bissell, R. Bedford, M. Crawford, *AIP Adv.* **2021**, *11*, 5.
- [24] R. V. Gorbachev, I. Riaz, R. R. Nair, R. Jalil, L. Britnell, B. D. Belle, E. W. Hill, K. S. Novoselov, K. Watanabe, T. Taniguchi, A. K. Geim, P. Blake, *Small* **2011**, *7*, 465.
- [25] D. Li, W. Gao, X. Sun, H. Yu, C. Liu, H. Yin, *Adv. Opt. Mater.* **2021**, *9*, 2100342.
- [26] X. Li, S. Sundaram, Y. El Gmili, T. Ayari, R. Puybaret, G. Patriarche, P. L. Voss, J. P. Salvestrini, A. Ougazzaden, *Cryst. Growth Des.* **2016**, *16*, 3409.
- [27] D. Chugh, J. Wong-Leung, L. Li, M. Lysevych, H. H. Tan, C. Jagadish, *2d Mater.* **2018**, *5*, 045018.
- [28] A. Bansal, M. Hilse, B. Huet, K. Wang, A. Kozhakhmetov, J. H. Kim, S. Bachu, N. Alem, R. Collazo, J. A. Robinson, *ACS Appl. Mater. Interfaces* **2021**, *13*, 54516.
- [29] E. N. Epie, D. N. Wijesundera, B. P. Tilakaratne, Q. Y. Chen, W. K. Chu, *Nucl. Instrum. Methods Phys. Res. B* **2016**, *371*, 303.
- [30] A. Gottscholl, M. Kianinia, V. Soltamov, S. Orlinskii, G. Mamin, C. Bradac, C. Kasper, K. Krambrock, A. Sperlich, M. Toth, I. Aharonovich, V. Dyakonov, *Nat. Mater.* **2020**, *19*, 540.
- [31] C. Qian, V. Villafañe, M. Schalk, G. V. Astakhov, U. Kentsch, M. Helm, P. Soubelet, N. P. Wilson, R. Rizzato, S. Mohr, A. W. Holleitner, D. B. Bucher, A. V. Stier, J. J. Finley, *Nano Lett.* **2022**, *22*, 5137.
- [32] S. Vaidya, X. Gao, S. Dikshit, I. Aharonovich, T. Li, *Adv. Phys.: X* **2023**, *8*, 2206049.
- [33] F. F. Murzakhonov, B. V. Yavkin, G. V. Mamin, S. B. Orlinskii, I. E. Mumdzhi, I. N. Gracheva, B. F. Gabbasov, A. N. Smirnov, V. Y. Davydov, V. A. Soltamov, *Nanomaterials* **2021**, *11*, 1373.
- [34] N.-J. Guo, W. Liu, Z.-P. Li, Y.-Z. Yang, S. Yu, Y. Meng, Z.-A. Wang, X.-D. Zeng, F.-F. Yan, Q. Li, J.-F. Wang, J.-S. Xu, Y.-T. Wang, J.-S. Tang, C.-F. Li, G.-C. Guo, *ACS Omega* **2022**, *7*, 1733.
- [35] X. Gao, S. Pandey, M. Kianinia, J. Ahn, P. Ju, I. Aharonovich, N. Shivaram, T. Li, *ACS Photonics* **2021**, *8*, 994.
- [36] M. Krečmarová, R. Canet-Albiach, H. Pashaei-Adl, S. Gorji, G. Muñoz-Matutano, M. Nešládek, J. P. Martínez-Pastor, J. F. Sánchez-Royo, *ACS Appl. Mater. Interfaces* **2021**, *13*, 46105.
- [37] S. Saha, Y.-C. Chang, T. H. Yang, A. Rice, A. Ghosh, W. You, M. Crawford, T.-H. Lu, Y.-W. Lan, S. Arafín, *Nanotechnology* **2022**, *33*, 215702.
- [38] N. V. Proscia, Z. Shotan, H. Jayakumar, P. Reddy, C. Cohen, M. Dollar, A. Alkauskas, M. Doherty, C. A. Meriles, V. M. Menon, *Optica* **2018**, *5*, 1128.
- [39] A. Kumar, C. Cholsuk, A. Zand, M. N. Mishuk, T. Matthes, F. Eilenberger, S. Suwanna, T. Vogl, *APL Mater.* **2023**, *11*, 7.
- [40] A. Bommer, C. Becher, *Nanophotonics* **2019**, *8*, 2041.
- [41] N. Mendelson, D. Chugh, J. R. Reimers, T. S. Cheng, A. Gottscholl, H. Long, C. J. Mellor, A. Zettl, V. Dyakonov, P. H. Beton, S. V. Novikov, C. Jagadish, H. H. Tan, M. J. Ford, M. Toth, C. Bradac, I. Aharonovich, *Nat. Mater.* **2021**, *20*, 321.
- [42] D. Zhong, S. Gao, M. Saccone, J. R. Greer, M. Bernardi, S. Nadj-Perge, A. Faraon, *Nano Lett.* **2024**, *24*, 1106.
- [43] C. Jara, T. Rauch, S. Botti, M. A. L. Marques, A. Norambuena, R. Coto, J. E. Castellanos-Águila, J. R. Maze, F. Muñoz, *J. Phys. Chem. A* **2021**, *125*, 1325.